

The effect of cryogenic thermal cycling on aging, rejuvenation, and mechanical properties of metallic glasses

Nikolai V. Priezjev^{1,2}

¹*Department of Mechanical and Materials Engineering,*

Wright State University, Dayton, OH 45435 and

²*National Research University Higher School of Economics, Moscow 101000, Russia*

(Dated: August 21, 2018)

Abstract

The structural relaxation, potential energy states, and mechanical properties of a model glass subjected to thermal cycling are investigated using molecular dynamics simulations. We study a non-additive binary mixture which is annealed with different cooling rates from the liquid phase to a low temperature well below the glass transition. The thermal treatment is applied by repeatedly heating and cooling the system at constant pressure, thus temporarily inducing internal stresses upon thermal expansion. We find that poorly annealed glasses are relocated to progressively lower levels of potential energy over consecutive cycles, whereas well annealed glasses can be rejuvenated at sufficiently large amplitudes of thermal cycling. Moreover, the lowest levels of potential energy after one hundred cycles are detected at a certain temperature amplitude for all cooling rates. The structural transition to different energy states is accompanied by collective nonaffine displacements of atoms that are organized into clusters, whose typical size becomes larger with increasing cooling rate or temperature amplitude. We show that the elastic modulus and the peak value of the stress overshoot exhibit distinct maxima at the cycling amplitude, which corresponds to the minimum of the potential energy. The simulation results indicate that the yielding peak as a function of the cycling amplitude for quickly annealed glasses represents a lower bound for the maximum stress in glasses prepared with lower cooling rates.

Keywords: glasses, deformation, temperature, yield stress, molecular dynamics simulations

I. INTRODUCTION

The development of novel processing routes that include thermal and mechanical treatments of metallic glasses is important for numerous engineering applications [1]. It is well accepted by now that in contrast to crystalline materials, amorphous solids can deform plastically via the so-called shear transformations, which involve only a few tens of atoms [2, 3]. Remarkably, recent experimental studies on metallic glasses have demonstrated that cryogenic thermal cycling can induce rejuvenation that leads to less relaxed states of higher energy and improved plasticity [4–8]. It was argued that atomic-scale structural rejuvenation upon thermal cycling might be caused by internal stresses that arise due to spatially heterogeneous thermal expansion of the amorphous material [9]. More recently, the probability distribution of local thermal expansion coefficients was estimated using atomistic simulations, and it was shown that internal stress can exceed the local yield stress and therefore trigger local shear transformations [10]. Similar to thermal agitation, it was originally demonstrated that a shear cycle can either overage or rejuvenate the glass depending on whether the strain amplitude is smaller or larger than the yield strain [11]. However, despite extensive efforts, the underlying mechanisms of structural relaxation or rejuvenation during thermomechanical treatments are still not fully understood.

In the last few years, the evolution of the potential energy, structural relaxation dynamics, and mechanical properties of glasses subjected to multiple shear cycles were examined using molecular dynamics (MD) simulations [12–26]. In particular, it was found that progressively lower energy states can be reached even for poorly annealed glasses by imposing a periodic shear deformation with the strain amplitude below yield [20, 24–26]. As the cycle number increases, the gradual decay of the potential energy at finite temperature is reflected in a reduction in size of transient clusters of atoms with relatively large nonaffine displacements [24, 25]. Upon approaching the yielding point from below, the potential energy decreases, while the storage modulus is slightly reduced [25]. Above the yielding transition, periodically sheared glasses settle at higher levels of potential energy, the loss modulus increases, and a shear band is formed after a number of cycles in sufficiently large systems [20, 21, 25]. However, the optimal parameter values for the strain amplitude, oscillation period, temperature, and cooling rate required to access a wide range of energy states and tune mechanical properties still need to be determined.

In this paper, the influence of thermal cycling on the potential energy and mechanical properties of binary glasses is studied using molecular dynamics simulations. The glasses are initially annealed across the glass transition with various cooling rates to a low temperature and then subjected to repeated heating and cooling cycles at constant pressure. We show that quickly annealed glasses reach lower levels of potential energy after one hundred thermal cycles, while slowly annealed glasses are rejuvenated at large temperature amplitudes. The results of numerical simulations indicate that the elastic modulus and the yield stress as a function of the cycling amplitude each exhibit a distinct maximum, which correlates well with the lowest potential energy level detected at the same amplitude.

This paper is organized as follows. The details of molecular dynamics simulations including parameter values, equilibration procedure, and temperature protocol are described in the next section. The results for the potential energy series, analysis of nonaffine displacements, and stress-strain response are presented in section III. A brief summary is provided in the last section.

II. DETAILS OF MD SIMULATIONS

The model glass studied in this paper is represented by the binary Lennard-Jones (LJ) mixture (80:20), which was originally developed by Kob and Andersen (KA) [27] to study the amorphous metal alloy Ni₈₀P₂₀ [28]. In this model, any two atoms of types $\alpha, \beta = A, B$ interact with each other via the truncated LJ potential:

$$V_{\alpha\beta}(r) = 4\varepsilon_{\alpha\beta} \left[\left(\frac{\sigma_{\alpha\beta}}{r} \right)^{12} - \left(\frac{\sigma_{\alpha\beta}}{r} \right)^6 \right], \quad (1)$$

where the interaction parameters for both types of atoms are specified as $\varepsilon_{AA} = 1.0$, $\varepsilon_{AB} = 1.5$, $\varepsilon_{BB} = 0.5$, $\sigma_{AB} = 0.8$, $\sigma_{BB} = 0.88$, and $m_A = m_B$ [27]. The LJ potential is truncated at the cutoff radius $r_{c,\alpha\beta} = 2.5\sigma_{\alpha\beta}$ to reduce computational cost. The reduced LJ units of length, mass, energy, and time were used to express physical quantities; more specifically, $\sigma = \sigma_{AA}$, $m = m_A$, $\varepsilon = \varepsilon_{AA}$, and $\tau = \sigma\sqrt{m/\varepsilon}$. The total number of atoms in the system is $N_{tot} = 60\,000$. A representative snapshot of the atomic configuration in the glassy phase is shown in Fig. 1. The equations of motion for each atom were solved numerically using the velocity Verlet algorithm [29] with the time step $\Delta t_{MD} = 0.005\tau$ using the open-source LAMMPS code [30].

In our setup, all atoms were initially placed in a periodic box and the system was allowed to equilibrate at a high-temperature liquid state in the NPT ensemble. Throughout the study, the pressure was kept constant, *i.e.*, $P = 0$. The temperature, denoted by T_{LJ} , was regulated using the Nosé-Hoover thermostat [30]. The computer glass transition temperature for the KA model is $T_c \approx 0.435 \varepsilon/k_B$ at the atomic density $\rho = \rho_A + \rho_B = 1.2 \sigma^{-3}$ [27]. Note that k_B denotes the Boltzmann constant. In the next step, the system was thermally annealed across the glass transition to the target temperature of $0.01 \varepsilon/k_B$ with cooling rates $10^{-2} \varepsilon/k_B \tau$, $10^{-3} \varepsilon/k_B \tau$, $10^{-4} \varepsilon/k_B \tau$, and $10^{-5} \varepsilon/k_B \tau$. Thus, the typical annealing time varies from about 100τ , which is only a couple of orders of magnitude greater than the atomic vibration time, to about $10^5 \tau$, which requires an efficient parallel code for the large system size [30]. Next, the annealed glasses were thermally cycled with the period $T = 10\,000 \tau$ over 100 cycles. During production runs, the system dimensions, temperature, pressure tensor, potential energy, as well as atom positions at the end of each cycle were saved for the post-processing analysis.

III. RESULTS

We first discuss the variation of the potential energy and glass density for samples annealed with cooling rates $10^{-2} \varepsilon/k_B \tau$, $10^{-3} \varepsilon/k_B \tau$, $10^{-4} \varepsilon/k_B \tau$, and $10^{-5} \varepsilon/k_B \tau$ to the low temperature of $0.01 \varepsilon/k_B$ and aged at this temperature and zero pressure for the time interval of $10^6 \tau$. The results are summarized in Fig. 2. As expected, more slowly annealed glasses at constant pressure attain lower levels of potential energy and become denser. Moreover, there is a noticeable decay in the potential energy for the poorly annealed glass (cooling rate $10^{-2} \varepsilon/k_B \tau$), whereas the potential energy for more slowly cooled glasses remains essentially constant during the time interval $10^6 \tau$. In what follows, these curves will be used as references for the analysis of potential energy series in thermally cycled glasses. Furthermore, as shown in the inset to Fig. 2, the glass density for the sample prepared with the fastest cooling rate of $10^{-2} \varepsilon/k_B \tau$ becomes slightly higher after $10^6 \tau$. Apart from thermal fluctuations, the density of the other samples remains unchanged. In the previous studies on the KA model, it was shown that when the system is quenched below the glass transition at constant volume, the potential energy exhibits a slow decay over time and the two-times correlation functions show a universal dependence on the waiting time, indicating progressively slower particle

dynamics [31, 32].

After the annealing procedure, the binary glasses were subjected to repeated thermal cycling, where the temperature was varied piecewise linearly from $0.01 \varepsilon/k_B$ to the maximum value and back to $0.01 \varepsilon/k_B$ over 100 cycles with the period $T = 10\,000 \tau$. An example of the temperature profiles measured during the first five cycles is presented in Fig. 3 for the amplitudes $0.2 \varepsilon/k_B$ and $0.4 \varepsilon/k_B$. It should be noted that since the simulations are performed at constant pressure ($P = 0$), the volume becomes expanded at elevated temperatures (not shown). The following temperature amplitudes were considered $T_{LJ} = 0.1 \varepsilon/k_B$, $0.2 \varepsilon/k_B$, $0.3 \varepsilon/k_B$, $0.4 \varepsilon/k_B$, and $0.435 \varepsilon/k_B$. Recall that the last value, $0.435 \varepsilon/k_B$, is the critical temperature of the KA model [27]. In this case, the system temporarily enters a state with sluggish dynamics and then is cooled back to $0.01 \varepsilon/k_B$ during each cycle.

The potential energy series for thermal cycling with various amplitudes are presented in Figs. 4, 5, 6, and 7 for the glasses annealed with cooling rates $10^{-2} \varepsilon/k_B \tau$, $10^{-3} \varepsilon/k_B \tau$, $10^{-4} \varepsilon/k_B \tau$, and $10^{-5} \varepsilon/k_B \tau$, respectively. For clarity, the data are only shown for the first and last 10 cycles. Note that the scale is the same in all four figures. It can be clearly observed in Figs. 4–7 that with increasing maximum cycling temperature, the amplitude of the potential energy variations becomes greater as the systems get thermally expanded and the interatomic distances increase on average. More importantly, however, one can notice that the potential energy minimum at the end of each cycle depends on the cooling rate, temperature amplitude, and the cycle number. Thus, in the case of the poorly annealed glass, shown in Fig. 4, the minima of the potential energy become progressively lower over consecutive cycles and remain below the energy level that corresponds to the glass aged at $T_{LJ} = 0.01 \varepsilon/k_B$. A more subtle feature of the potential energy variation during the last cycle can be identified in the inset to Fig. 4; namely, the lowest energy minimum, $U \approx -8.34 \varepsilon$, is attained at the cycling amplitude of $0.3 \varepsilon/k_B$.

Similar patterns for the potential energy series can be observed for more slowly annealed glasses (cooling rates $10^{-3} \varepsilon/k_B \tau$ and $10^{-4} \varepsilon/k_B \tau$) shown in Figs. 5 and 6, except that thermal cycling with the amplitude $0.1 \varepsilon/k_B$ results in the energy minima being only slightly lower than the energy levels of the glasses aged at $T_{LJ} = 0.01 \varepsilon/k_B$. Furthermore, as shown in Fig. 7, the well annealed glass (cooling rate $10^{-5} \varepsilon/k_B \tau$) attains nearly the same energy minima when cycled with the amplitudes $0.1 \varepsilon/k_B$ and $0.2 \varepsilon/k_B$, while the lowest energy

minimum, $U \approx -8.35\varepsilon$, is reached at $0.3\varepsilon/k_B$. Interestingly, the well annealed sample becomes rejuvenated at the cycling amplitude of $0.4\varepsilon/k_B$, as its potential energy minimum is slightly higher than the energy level for the glass aged at $T_{LJ} = 0.01\varepsilon/k_B$ (see inset to Fig. 7). Overall, the important conclusion from Figs. 4–7 is that, despite the energy levels for annealed glasses in Fig. 2 being distinctly different, the energy minima for glasses cycled with amplitude $0.3\varepsilon/k_B$ over 100 cycles are nearly the same; $U(100T)$ only slightly decreases from $U \approx -8.34\varepsilon$ for the poorly annealed glass to $U \approx -8.35\varepsilon$ for the well annealed glass.

Structural relaxation processes in thermally cycled glasses can be studied by analyzing the so-called nonaffine displacements, which represent a deviation from the local linear deformation of the material. Numerically, the nonaffine measure associated with an atom i is computed via the transformation matrix \mathbf{J}_i that describes a linear transformation of a small group of neighboring atoms during the time interval Δt , while at the same time minimizing the quantity $D^2(t, \Delta t)$ as follows [33]:

$$D^2(t, \Delta t) = \frac{1}{N_i} \sum_{j=1}^{N_i} \left\{ \mathbf{r}_j(t + \Delta t) - \mathbf{r}_i(t + \Delta t) - \mathbf{J}_i [\mathbf{r}_j(t) - \mathbf{r}_i(t)] \right\}^2, \quad (2)$$

where the sum is over nearest neighbors that are located closer than 1.5σ to the i -th atom. Recently, the analysis of spatial configurations of atoms with large nonaffine displacements was carried out for cyclically sheared [17, 19, 21, 24, 25] and compressed [34] glasses. In particular, it was demonstrated that after a certain number of shear cycles, the yielding transition at finite temperature is accompanied by the formation of a system-spanning shear band of large nonaffine displacements in both well [21] and poorly [25] annealed glasses. On the other hand, below the yield point, binary glasses start to deform reversibly after transient cycles and nonaffine displacements become organized into compact clusters [17, 19, 21, 24, 25, 34].

We next discuss nonaffine displacements in thermally cycled glasses for two limiting cases of the fastest $10^{-2}\varepsilon/k_B\tau$ and slowest $10^{-5}\varepsilon/k_B\tau$ cooling rates. The representative snapshots of atoms with large nonaffine displacements during the first, second, 10-th, and 100-th cycles are presented in Figs. 8, 9, 10, and 11 for two cycling amplitudes $0.2\varepsilon/k_B$ and $0.3\varepsilon/k_B$. In our analysis, the nonaffine measure was computed for all atoms during the time interval $\Delta t = T$, and only atoms with $D^2 > 0.04\sigma^2$ are displayed in Figs. 8–11. For comparison, the typical cage size is about 0.1σ . It can be seen in Figs. 8 and 9 that most of the atoms in the poorly

annealed glass (cooling rate $10^{-2}\varepsilon/k_B\tau$) undergo large nonaffine displacements during the first couple of cycles, leading to irreversible atom displacements and lower potential energy states (see Fig. 4). This process continues for 100 cycles, although the typical size of clusters of nonaffine displacements is gradually reduced over consecutive cycles. Notice that the number of atoms with large nonaffine displacements after the 100-th cycle is smaller for the amplitude $0.2\varepsilon/k_B$ than for $0.3\varepsilon/k_B$, which suggests that internal stresses due to thermal expansion are smaller in the former case.

By contrast, the typical size of clusters of atoms with large nonaffine displacements for the well annealed glass (cooling rate $10^{-5}\varepsilon/k_B\tau$) depends only weakly on the cycle number for both temperature amplitudes $0.2\varepsilon/k_B$ and $0.3\varepsilon/k_B$, shown in Figs. 10 and 11. Similar to the poorly annealed sample, the clusters in the well annealed glass are larger for the thermal amplitude $0.3\varepsilon/k_B$ than for $0.2\varepsilon/k_B$. Interestingly, despite the appearance of small-size clusters at the cycling amplitude of $0.2\varepsilon/k_B$ in Fig. 10, the potential energy minima at the amplitude of $0.2\varepsilon/k_B$ remain nearly equal to the energy level of the glass aged at the constant temperature $T_{LJ} = 0.01\varepsilon/k_B$ (see inset to Fig. 7). We further comment that during thermal cycling with amplitude $0.4\varepsilon/k_B$, most of the atoms have $D^2 > 0.04\sigma^2$ after one period T for any cooling rate or cycle number (not shown). It should be emphasized, however, that only the well annealed sample, prepared with the cooling rate of $10^{-5}\varepsilon/k_B\tau$, acquires a higher energy state after 100 cycles with amplitude $0.4\varepsilon/k_B$ (see insets to Figs. 4–7). Finally, the spatial configurations of atoms with large nonaffine displacements in glasses prepared with intermediate cooling rates, $10^{-3}\varepsilon/k_B\tau$ and $10^{-4}\varepsilon/k_B\tau$, are roughly extrapolated between the two limiting cases, and they are omitted here for brevity.

We find that the thermal treatment of binary glasses can significantly affect their mechanical properties. The stress-strain curves for different cycling amplitudes are presented in Fig. 12 for cooling rates $10^{-2}\varepsilon/k_B\tau$, $10^{-3}\varepsilon/k_B\tau$, $10^{-4}\varepsilon/k_B\tau$, and $10^{-5}\varepsilon/k_B\tau$. All samples were strained with the rate $\dot{\varepsilon}_{xx} = 10^{-5}\tau^{-1}$ after 100 thermal cycles. For reference, the data for glasses aged at the constant temperature $T_{LJ} = 0.01\varepsilon/k_B$ during the time interval $10^6\tau = 100T$ are also reported in Fig. 12. As expected, upon decreasing cooling rate, a pronounced peak at the yield strain is developed for glasses aged at $T_{LJ} = 0.01\varepsilon/k_B$. Furthermore, it can be seen in Fig. 12 that the dependence of the yield stress on the cycling amplitude is nonmonotonic, and the highest peak appears at $T_{LJ} = 0.3\varepsilon/k_B$ for all cooling

rates. This behavior correlates well with the occurrence of the lowest minima of the potential energy at the amplitude of $0.3 \varepsilon/k_B$ shown in the insets to Figs. 4–7.

The summary of the data for the yielding peak, σ_Y , the elastic modulus, E , and the potential energy minimum, $U(100T)$, as a function of the cycling amplitude is presented in Fig. 13. As is evident, both σ_Y and E increase, while $U(100T)$ is reduced, when T_{LJ} approaches $0.3 \varepsilon/k_B$ from below. It can be observed that at temperature amplitudes above $0.3 \varepsilon/k_B$, the values of the yielding peak and the potential energy minimum after 100 cycles are only weakly dependent on the cooling rate. Note also that the yielding peak for the rejuvenated glass (cooling rate $10^{-5} \varepsilon/k_B \tau$) at the cycling amplitude $0.4 \varepsilon/k_B$ is smaller than σ_Y for the same sample aged at $T_{LJ} = 0.01 \varepsilon/k_B$. This behavior correlates well with the dependence of $U(100T)$ for the well annealed sample, shown in the inset (a) to Fig. 13. Furthermore, the numerical results in Fig. 13 suggest that the peak value of the stress overshoot for poorly annealed glasses that are cycled with amplitudes below $0.3 \varepsilon/k_B$ represents a lower bound for σ_Y measured in more slowly annealed glasses. Plotted in the inset (b) to Fig. 13, the elastic modulus shows a similar dependence on the thermal amplitude and cooling rate, although the data appear to be more scattered at large amplitudes. Altogether, these results demonstrate that the elastic modulus and the stress overshoot increase in binary glasses subjected to multiple periods of heating and cooling up to a certain temperature. The effect is most pronounced at the maximum temperature $T_{LJ} \approx 0.69 T_c$.

IV. CONCLUSIONS

In summary, molecular dynamics simulations were carried out to study structural relaxation and mechanical properties of a model glass after thermal cycling with different amplitudes. We considered a binary Lennard-Jones mixture, which was initially annealed from the liquid state to a temperature well below the glass transition. With increasing cooling rate, the glasses settle into more shallow potential energy minima and become less dense. After annealing, the thermal treatment was imposed during one hundred cycles of heating and cooling at constant pressure. We found that depending on the cooling rate and cycling amplitude, the glasses can be either overaged or rejuvenated by periodic temperature variations. Thus, the potential energy in quickly annealed glasses decreases during thermal cycling, while the potential energy in slowly annealed glasses increases at large cycling am-

plitudes. It was further shown that the lowest energy minima are attained at a particular temperature amplitude for quickly and slowly annealed glasses. In all cases, the structural changes leading to different energy states occur via collective nonaffine displacements of atoms, and the typical size of clusters of mobile atoms is reduced with decreasing cooling rate or temperature amplitude and with increasing cycle number. In turn, the mechanical properties were probed via uniaxial tensile loading at constant pressure after the thermal treatment. The simulation results demonstrated that the elastic modulus and the peak value of the stress overshoot become larger with increasing cycling amplitude up to about two-thirds of the glass transition temperature. In this range, the variation of the yield peak as a function of the temperature amplitude for quickly annealed glasses provides a lower bound for the maximum stress in more slowly annealed glasses.

Acknowledgments

Financial support from the National Science Foundation (CNS-1531923) is gratefully acknowledged. The article was prepared within the framework of the Basic Research Program at the National Research University Higher School of Economics (HSE) and supported within the framework of a subsidy by the Russian Academic Excellence Project ‘5-100’. The molecular dynamics simulations were performed using the LAMMPS numerical code developed at Sandia National Laboratories [30]. Computational work in support of this research was performed at Wright State University’s Computing Facility and the Ohio Supercomputer Center.

-
- [1] J. J. Kruzic, Bulk Metallic Glasses as Structural Materials: A Review, *Adv. Eng. Mater.* **18**, 1308 (2016).
 - [2] A. S. Argon, Plastic deformation in metallic glasses, *Acta Metall.* **27**, 47 (1979).
 - [3] F. Spaepen, A microscopic mechanism for steady state inhomogeneous flow in metallic glasses, *Acta Metall.* **25**, 407 (1977).
 - [4] S. V. Ketov, Y. H. Sun, S. Nachum, Z. Lu, A. Checchi, A. R. Beraldin, H. Y. Bai, W. H. Wang, D. V. Louzguine-Luzgin, M. A. Carpenter, and A. L. Greer, Rejuvenation of metallic glasses by non-affine thermal strain, *Nature* **524**, 200 (2015).

- [5] W. Song, X. Meng, Y. Wu, D. Cao, H. Wang, X. Liu, X. Wang, and Z. Lu, Improving plasticity of the $Zr_{46}Cu_{46}Al_8$ bulk metallic glass via thermal rejuvenation, *Science Bulletin* **63**, 840 (2018).
- [6] D. Grell, F. Dabrock, and E. Kerscher, Cyclic cryogenic pretreatments influencing the mechanical properties of a bulk glassy Zr-based alloy, *Fatigue Fract. Eng. Mater. Struct.* **41**, 1330 (2018).
- [7] W. Guoa, R. Yamada, and J. Saida, Rejuvenation and plasticization of metallic glass by deep cryogenic cycling treatment, *Intermetallics* **93**, 141 (2018).
- [8] S. V. Ketov, A. S. Trifonov, Y. P. Ivanov, A. Yu. Churyumov, A. V. Lubenchenko, A. A. Batrakov, J. Jiang, D. V. Louzguine-Luzgin, J. Eckert, J. Orava, and A. L. Greer, On cryothermal cycling as a method for inducing structural changes in metallic glasses, *NPG Asia Materials* **10**, 137 (2018).
- [9] T. C. Hufnagel, Metallic glasses: Cryogenic rejuvenation, *Nature Materials* **14**, 867 (2015).
- [10] B. Shang, P. Guan, and J.-L. Barrat, Role of thermal expansion heterogeneity in the cryogenic rejuvenation of metallic glasses, arXiv:1807.00760 (2018).
- [11] D. J. Lacks and M. J. Osborne, Energy landscape picture of overaging and rejuvenation in a sheared glass, *Phys. Rev. Lett.* **93**, 255501 (2004).
- [12] N. V. Priezjev, Heterogeneous relaxation dynamics in amorphous materials under cyclic loading, *Phys. Rev. E* **87**, 052302 (2013).
- [13] D. Fiocco, G. Foffi, and S. Sastry, Oscillatory athermal quasistatic deformation of a model glass, *Phys. Rev. E* **88**, 020301(R) (2013).
- [14] I. Regev, T. Lookman, and C. Reichhardt, Onset of irreversibility and chaos in amorphous solids under periodic shear, *Phys. Rev. E* **88**, 062401 (2013).
- [15] N. V. Priezjev, Dynamical heterogeneity in periodically deformed polymer glasses, *Phys. Rev. E* **89**, 012601 (2014).
- [16] I. Regev, J. Weber, C. Reichhardt, K. A. Dahmen, and T. Lookman, Reversibility and criticality in amorphous solids, *Nat. Commun.* **6**, 8805 (2015).
- [17] N. V. Priezjev, Reversible plastic events during oscillatory deformation of amorphous solids, *Phys. Rev. E* **93**, 013001 (2016).
- [18] T. Kawasaki and L. Berthier, Macroscopic yielding in jammed solids is accompanied by a non-equilibrium first-order transition in particle trajectories, *Phys. Rev. E* **94**, 022615 (2016).

- [19] N. V. Priezjev, Nonaffine rearrangements of atoms in deformed and quiescent binary glasses, *Phys. Rev. E* **94**, 023004 (2016).
- [20] P. Leishangthem, A. D. S. Parmar, and S. Sastry, The yielding transition in amorphous solids under oscillatory shear deformation, *Nat. Commun.* **8**, 14653 (2017).
- [21] N. V. Priezjev, Collective nonaffine displacements in amorphous materials during large-amplitude oscillatory shear, *Phys. Rev. E* **95**, 023002 (2017).
- [22] M. Fan, M. Wang, K. Zhang, Y. Liu, J. Schroers, M. D. Shattuck, and C. S. O'Hern, The effects of cooling rate on particle rearrangement statistics: Rapidly cooled glasses are more ductile and less reversible, *Phys. Rev. E* **95**, 022611 (2017).
- [23] S. Dagois-Bohy, E. Somfai, B. P. Tighe, and M. van Hecke, Softening and yielding of soft glassy materials, *Soft Matter* **13**, 9036 (2017).
- [24] N. V. Priezjev, Molecular dynamics simulations of the mechanical annealing process in metallic glasses: Effects of strain amplitude and temperature, *J. Non-Cryst. Solids* **479**, 42 (2018).
- [25] N. V. Priezjev, The yielding transition in periodically sheared binary glasses at finite temperature, *Comput. Mater. Sci.* **150**, 162 (2018).
- [26] P. Das, A. D. S. Parmar, and S. Sastry, Annealing glasses by cyclic shear deformation, *arXiv:1805.12476* (2018).
- [27] W. Kob and H. C. Andersen, Testing mode-coupling theory for a supercooled binary Lennard-Jones mixture: The van Hove correlation function, *Phys. Rev. E* **51**, 4626 (1995).
- [28] T. A. Weber and F. H. Stillinger, Local order and structural transitions in amorphous metal-metalloid alloys, *Phys. Rev. B* **31**, 1954 (1985).
- [29] M. P. Allen and D. J. Tildesley, *Computer Simulation of Liquids* (Clarendon, Oxford, 1987).
- [30] S. J. Plimpton, Fast parallel algorithms for short-range molecular dynamics, *J. Comp. Phys.* **117**, 1 (1995).
- [31] W. Kob and J.-L. Barrat, Aging Effects in a Lennard-Jones Glass, *Phys. Rev. Lett.* **78**, 4581 (1997).
- [32] W. Kob and J.-L. Barrat, Fluctuations, response and aging dynamics in a simple glass-forming liquid out of equilibrium, *Eur. Phys. J. B* **13**, 319 (2000).
- [33] M. L. Falk and J. S. Langer, Dynamics of viscoplastic deformation in amorphous solids, *Phys. Rev. E* **57**, 7192 (1998).
- [34] N. V. Priezjev, Slow relaxation dynamics in binary glasses during stress-controlled, tension-

compression cyclic loading, *Comput. Mater. Sci.* **153**, 235 (2018).

Figures

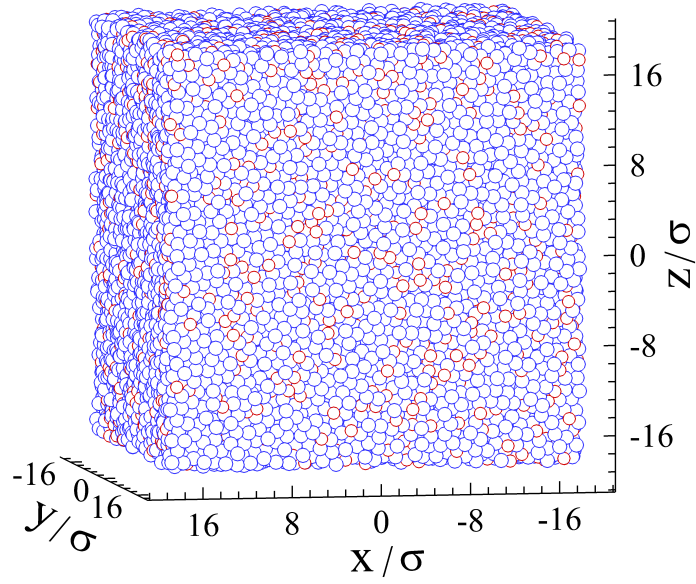


FIG. 1: (Color online) An atomic configuration of the binary Lennard-Jones glass ($N_{tot} = 60\,000$) after isobaric quench from a liquid state to the temperature $T_{LJ} = 0.01 \varepsilon/k_B$ with the cooling rate of $10^{-3} \varepsilon/k_B \tau$. Atoms of types A and B , denoted by blue and red spheres, are not shown to scale.

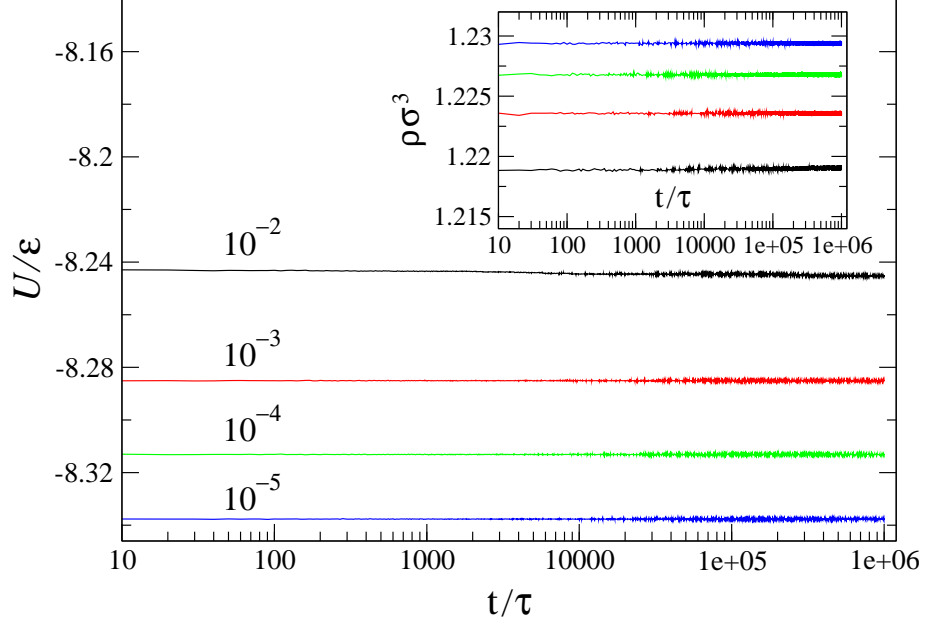


FIG. 2: (Color online) The potential energy during aging process at $T_{LJ} = 0.01 \varepsilon/k_B$ in samples prepared with cooling rates $10^{-2}\varepsilon/k_B\tau$ (black curve), $10^{-3}\varepsilon/k_B\tau$ (red curve), $10^{-4}\varepsilon/k_B\tau$ (green curve), and $10^{-5}\varepsilon/k_B\tau$ (blue curve). The inset shows the evolution of the glass density for the same samples.

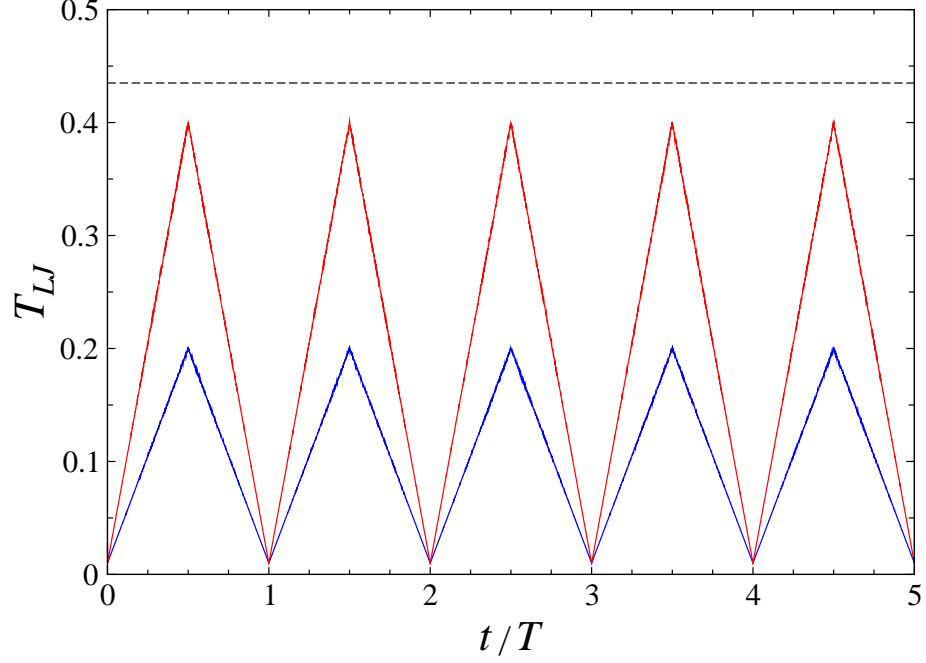


FIG. 3: (Color online) The variation of temperature T_{LJ} (in units of ε/k_B) during the first five periods, $T = 10\,000\tau$, for the temperature amplitudes $0.2\varepsilon/k_B$ (blue curve) and $0.4\varepsilon/k_B$ (red curve). The data are taken in the sample initially prepared with the cooling rate of $10^{-4}\varepsilon/k_B\tau$. The black dashed line denotes the critical temperature of $0.435\varepsilon/k_B$.

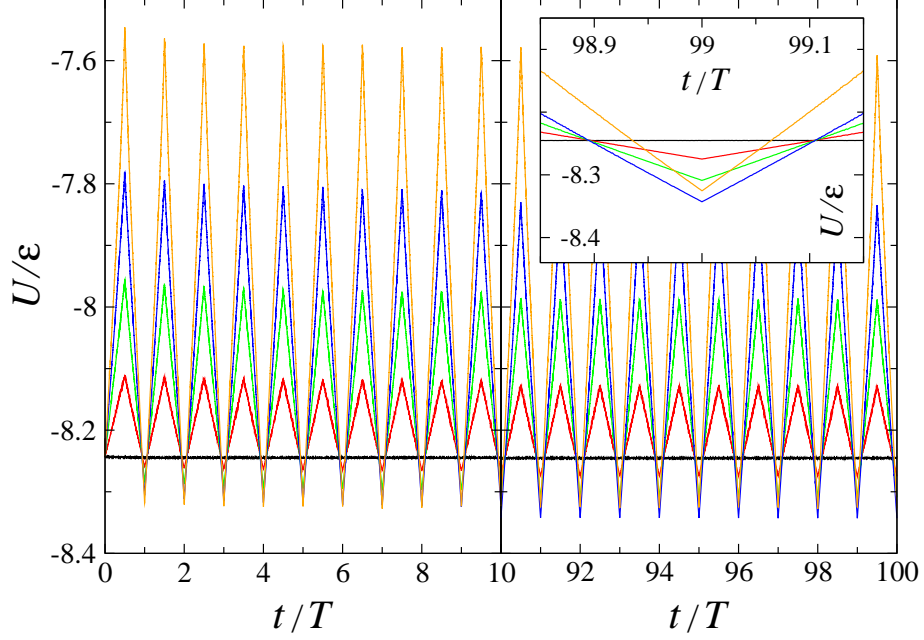


FIG. 4: (Color online) The potential energy during the first 10 (left panel) and the last 10 (right panel) thermal cycles with amplitudes $0.1\varepsilon/k_B$ (red), $0.2\varepsilon/k_B$ (green), $0.3\varepsilon/k_B$ (blue), and $0.4\varepsilon/k_B$ (orange). The black curve denotes the data for the same sample aged at the temperature of $0.01\varepsilon/k_B$. The cooling rate is $10^{-2}\varepsilon/k_B\tau$. The inset shows an enlarged view of the same data at $t = 99T$.

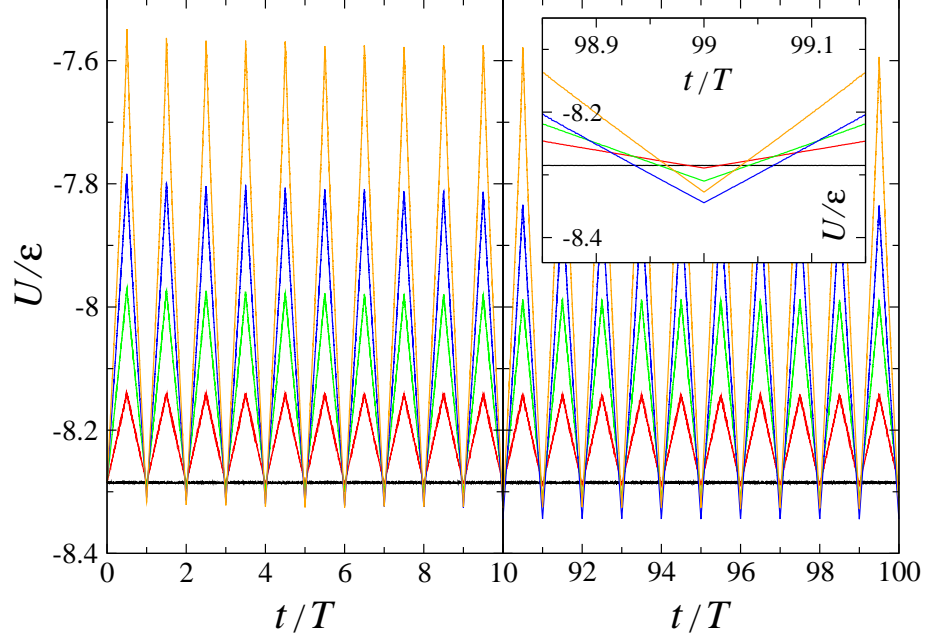


FIG. 5: (Color online) The potential energy series for the glass annealed with the cooling rate of $10^{-3}\varepsilon/k_B\tau$ and thermally cycled with amplitudes $0.1\varepsilon/k_B$ (red), $0.2\varepsilon/k_B$ (green), $0.3\varepsilon/k_B$ (blue), and $0.4\varepsilon/k_B$ (orange). The data at the temperature of $0.01\varepsilon/k_B$ are denoted by the black line. An enlarged view of the same data is shown in the inset.

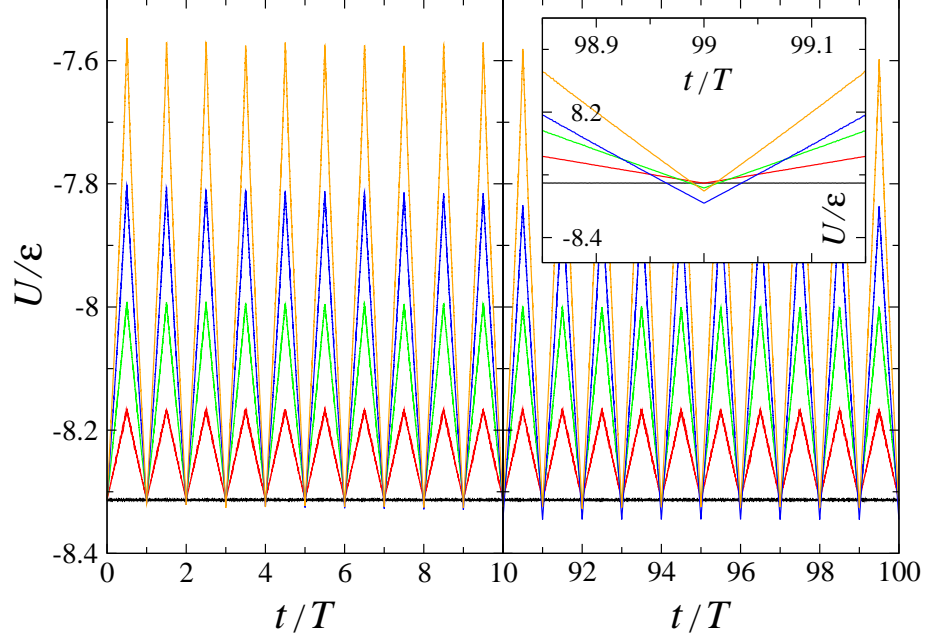


FIG. 6: (Color online) The variation of the potential energy for the sample prepared with the cooling rate of $10^{-4}\varepsilon/k_B\tau$ and cycled with thermal amplitudes $0.1\varepsilon/k_B$ (red), $0.2\varepsilon/k_B$ (green), $0.3\varepsilon/k_B$ (blue), and $0.4\varepsilon/k_B$ (orange). The black line denotes the potential energy at $T_{LJ} = 0.01\varepsilon/k_B$. The inset shows an expanded view of the same data during the last cycle.

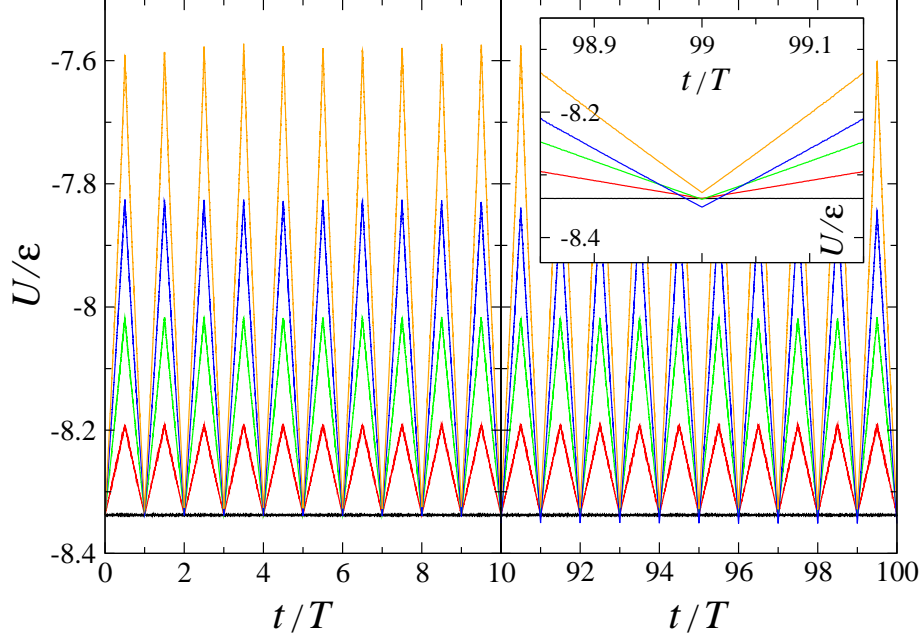


FIG. 7: (Color online) The potential energy for the well annealed glass (cooling rate $10^{-5}\varepsilon/k_B\tau$) and temperature amplitudes $0.1\varepsilon/k_B$ (red), $0.2\varepsilon/k_B$ (green), $0.3\varepsilon/k_B$ (blue), and $0.4\varepsilon/k_B$ (orange). The potential energy at $T_{LJ} = 0.01\varepsilon/k_B$ is indicated by the black line. A close-up view of the same data at $t = 99T$ is shown in the inset.

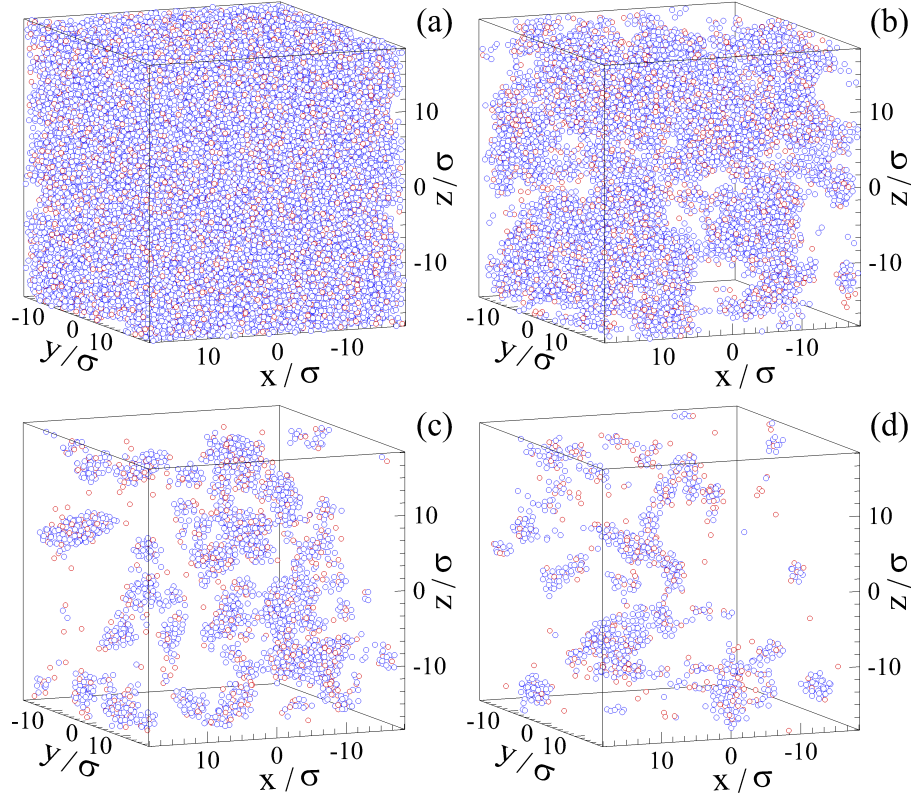


FIG. 8: (Color online) Spatial configurations of atoms with large nonaffine measure (a) $D^2(0, T) > 0.04\sigma^2$, (b) $D^2(T, T) > 0.04\sigma^2$, (c) $D^2(9T, T) > 0.04\sigma^2$, and (d) $D^2(99T, T) > 0.04\sigma^2$. The cooling rate is $10^{-2}\varepsilon/k_B\tau$ and the amplitude of thermal cycling is $0.2\varepsilon/k_B$.

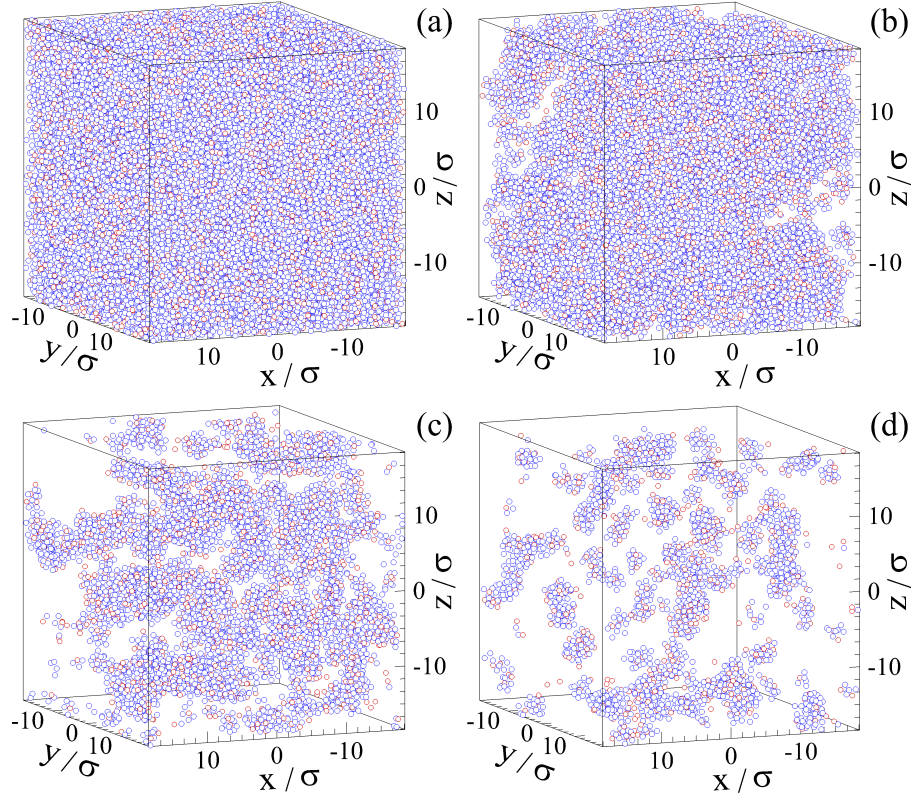


FIG. 9: (Color online) Atomic configurations of the binary glass prepared with the cooling rate of $10^{-2}\varepsilon/k_B\tau$ and subjected to thermal cycling with the amplitude $0.3\varepsilon/k_B$. The nonaffine measures are (a) $D^2(0, T) > 0.04\sigma^2$, (b) $D^2(T, T) > 0.04\sigma^2$, (c) $D^2(9T, T) > 0.04\sigma^2$, and (d) $D^2(99T, T) > 0.04\sigma^2$.

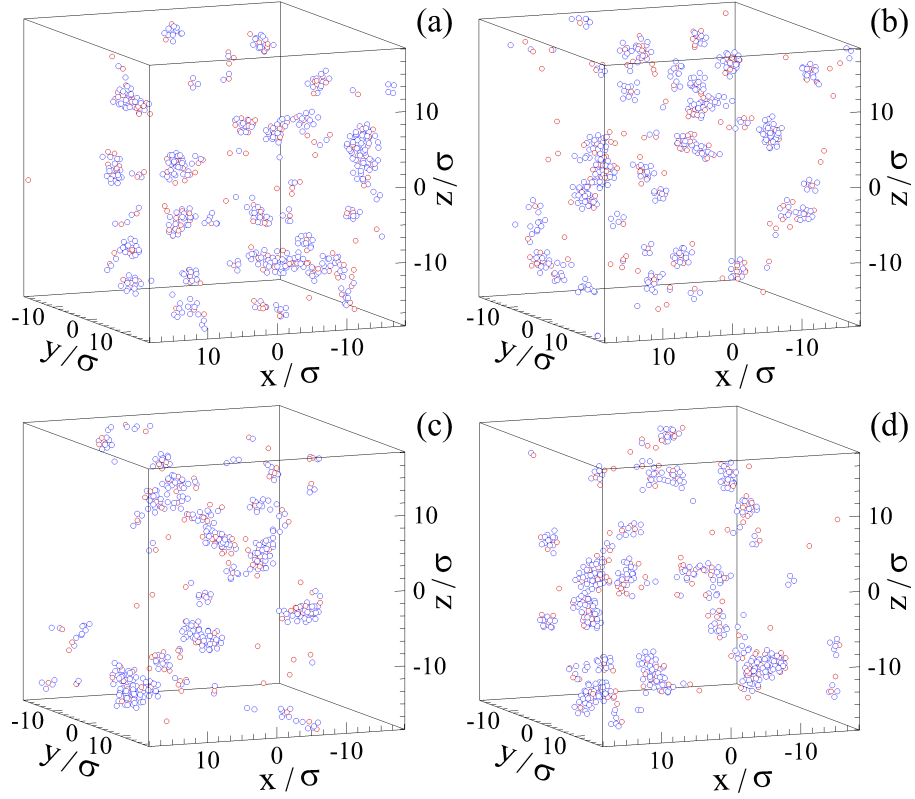


FIG. 10: (Color online) Positions of atoms with large nonaffine displacements (a) $D^2(0, T) > 0.04 \sigma^2$, (b) $D^2(T, T) > 0.04 \sigma^2$, (c) $D^2(9T, T) > 0.04 \sigma^2$, and (d) $D^2(99T, T) > 0.04 \sigma^2$. The sample was initially cooled with the rate of $10^{-5} \varepsilon / k_B \tau$ and then thermally cycled with the amplitude of $0.2 \varepsilon / k_B$.

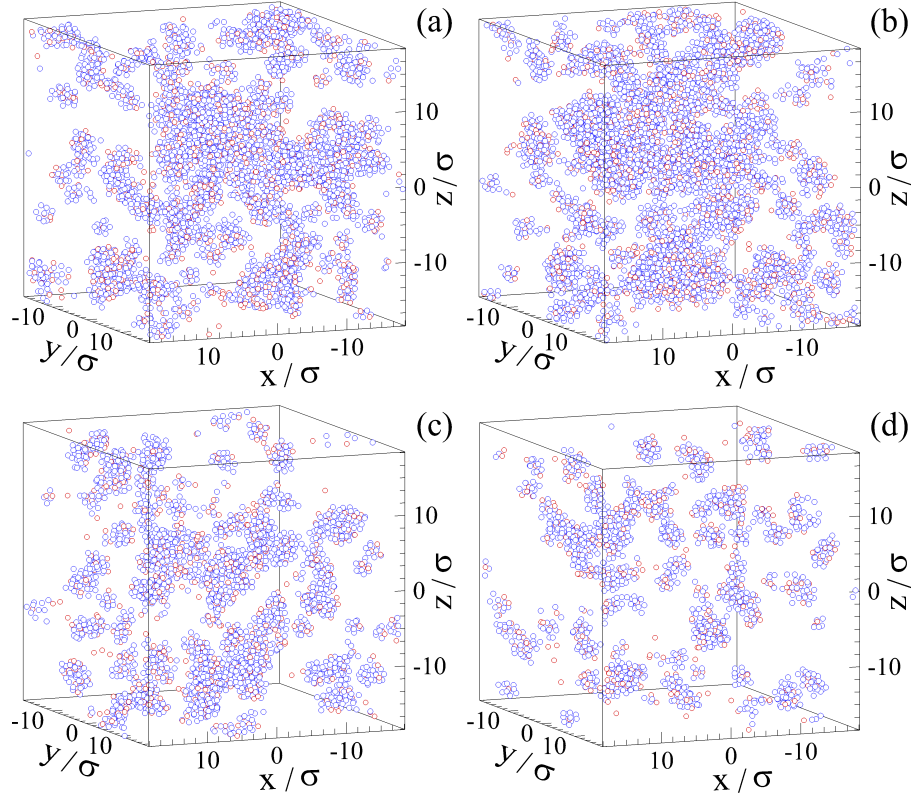


FIG. 11: (Color online) Snapshots of atoms with relatively large nonaffine displacements (a) $D^2(0, T) > 0.04\sigma^2$, (b) $D^2(T, T) > 0.04\sigma^2$, (c) $D^2(9T, T) > 0.04\sigma^2$, and (d) $D^2(99T, T) > 0.04\sigma^2$. The glass is thermally cycled with the amplitude of $0.3\varepsilon/k_B$ and it is initially prepared with the rate of cooling $10^{-5}\varepsilon/k_B\tau$.

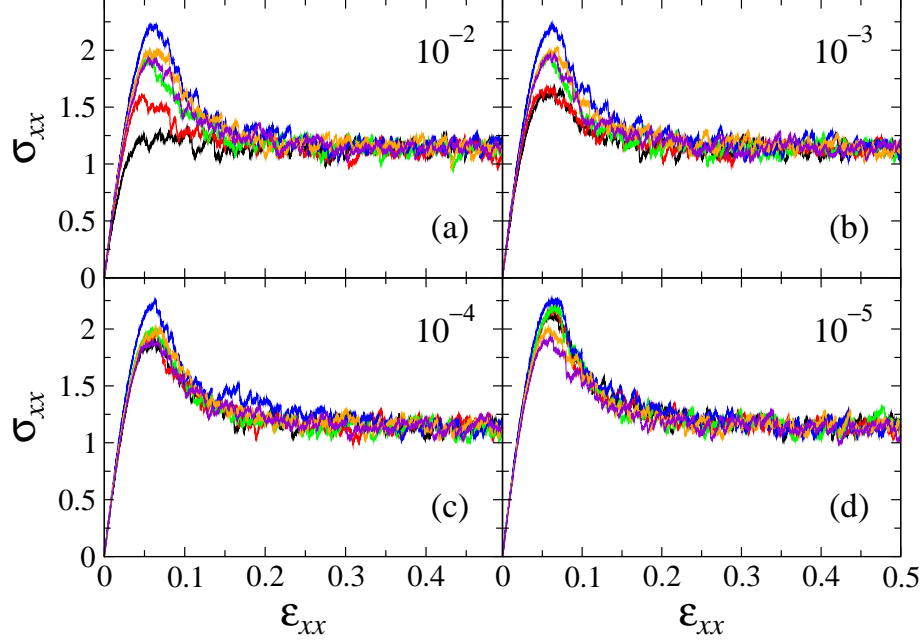


FIG. 12: (Color online) The dependence of tensile stress σ_{xx} (in units of $\varepsilon\sigma^{-3}$) as a function of strain for samples obtained with cooling rates (a) $10^{-2}\varepsilon/k_B\tau$, (b) $10^{-3}\varepsilon/k_B\tau$, (c) $10^{-4}\varepsilon/k_B\tau$, and (d) $10^{-5}\varepsilon/k_B\tau$. The stress response for glasses aged at the constant temperature of $0.01\varepsilon/k_B$ is denoted by the black curves. The stress-strain curves are computed after 100 periods of thermal cycling with the amplitudes $0.1\varepsilon/k_B$ (red), $0.2\varepsilon/k_B$ (green), $0.3\varepsilon/k_B$ (blue), $0.4\varepsilon/k_B$ (orange), and $0.435\varepsilon/k_B$ (violet). The strain rate is $\dot{\varepsilon}_{xx} = 10^{-5}\tau^{-1}$.

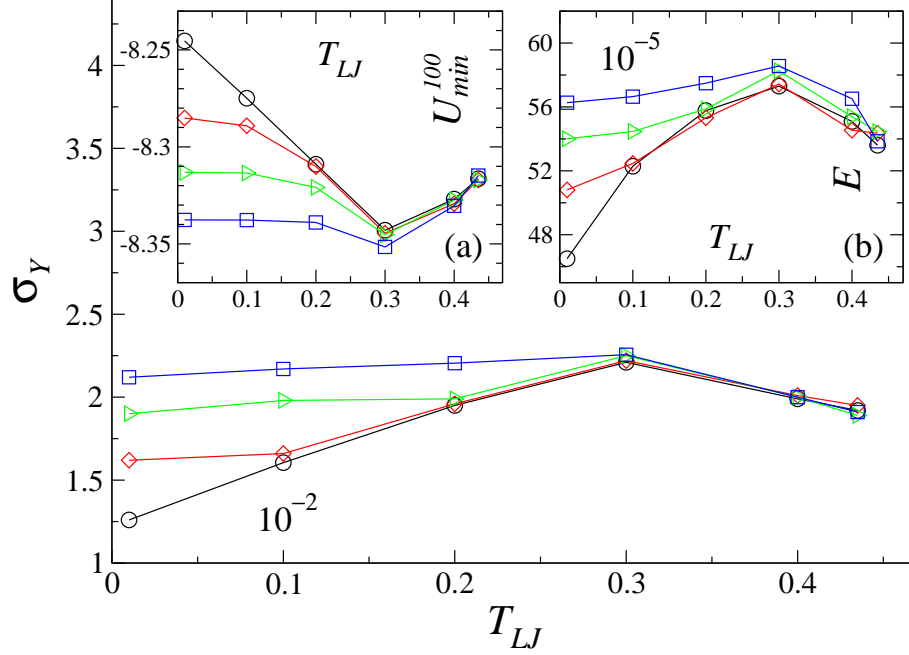


FIG. 13: (Color online) The peak value of the stress overshoot σ_Y (in units of $\epsilon\sigma^{-3}$) versus the amplitude of thermal cycling for cooling rates $10^{-2}\epsilon/k_B\tau$ (black curve), $10^{-3}\epsilon/k_B\tau$ (red curve), $10^{-4}\epsilon/k_B\tau$ (green curve), and $10^{-5}\epsilon/k_B\tau$ (blue curve). The minimum of the potential energy after 100 cycles is shown in the inset (a) for different cooling rates (the colorcode is the same). The inset (b) shows the elastic modulus E (in units of $\epsilon\sigma^{-3}$) as a function of the temperature amplitude for the same samples.